European Journal of Mechanics A/Solids 66 (2017) 201–211

Contents lists available at ScienceDirect

European Journal of Mechanics A/Solids

journal homepage: www.elsevier.com/locate/ejmsol

Instability load evaluation of shallow imperfection-sensitive structures by form and interaction parameters

F. Bazzucchi*, A. Manuello, A. Carpinteri

Politecnico di Torino, DISEG Department of Structural, Geotechnical and Building Engineering, Corso Duca degli Abruzzi, 24, 10129, Torino, Italy

ARTICLE INFO

Article history:
Received 27 March 2017
Received in revised form
10 July 2017
Accepted 15 July 2017
Available online 20 July 2017

Keywords:
Buckling
Coupled instability
Imperfection sensitivity
Pull-in
Snap-through
Interaction curve
Nonlinear bifurcation

ABSTRACT

In terms of the interaction between buckling and snap-through for shallow structures affected by geometrical imperfections results have shown that, after the nonlinear bifurcation, load reductions occurs accompanied with a predictable tendency. In order to do it, the tracing of *interaction domains* and *interaction curves* presented in recent papers by the same Authors, has been proposed. In this study, every simple structural arrangement has been analyzed with regards to different shallowness ratios, slenderness, restraining conditions and imperfection patterns. It has been observed how the driving parameters could be led back to two original interaction (Δ) and form (Ω) factors. This procedure could shed new light on the application of the more burdensome imperfection pattern for the instability of geometrically nonlinear structures. Possible implications of these results have been presented, with a special attention to sensors and structural identification. The study accomplished numerous numerical simulations and showed good agreement with the theoretical expected results.

1. Introduction

Improving the efficiency of constructions by reducing their weight and material consumption is a major trend in Structural Engineering. This aim can be achieved through the adoption of new solutions, materials and by the rationalizing of the existing ones. It has been possible to observe, over the last twenty years, the construction of many lightweight structures, such as long-span roofs, laced columns, stiffened plates, thin-walled members etc … For all these structural systems, the checking for stability is essential.

Main focuses of Structural Instability research are the improvement of the solutions and a better knowledge of the behavior of the structures. This lead to an important reduction of the dimensions of structural members, which in its turn increases the slenderness of structures. After the first Koiter's studies (Koiter, 1976) it was possible to observe that the loss of stability, in many practical cases, often takes place with the occurrence of two or more eigenmodes at coincident, or nearly coincident, critical loads. This situation arises during attempts to optimize structures for stability by choosing that appropriate configuration which allows to have the same critical loads for the main buckling modes (*simultaneous buckling design principle* (Bleich, 1952)). Thompson (1972) observed that the main characteristic of these instabilities forms is an increased sensitivity to geometrical and mechanical imperfections. As a consequence, a more significant decrease in the critical load than in the case of single instabilities exists.

At the same times, many Authors (i.e. (Bradford and Hancock, 1984), (Grimaldi and Pignataro, 1979), (Maquoi and Massonnet, 1976)) highlighted the interaction between local and global instability, treating the mathematical problem as an interactive buckling. As a result of these multiple studies, strong effort has been expended at the end of last century to understand and solve the problem of interactive buckling. International organizations (like IUTAM or EUROMECH) supported a large number of studies, most of them based on the theories of Koiter (1970) and of Chilver's (Chilver, 1967) as fundamentals. The jointed work found its acme in the "First Conference of Coupled Instability", held in Timisoara in 1994. Main results and contributions have been collected by Gioncu in a detailed report of the conference (Gioncu, 1994), (Gioncu et al., 1992). Even if many remarkable achievements have been reached, there was also many inexplicable aspects, specially on the theoretical quantification of the maximum load reduction for a given imperfection (Gioncu, 1994). Coupled instability generated considerable recent research interest and still remains one of the most attractive topics in the field of Stability of Metal Structures.

* Corresponding author.
E-mail address: fabio.bazzucchi@polito.it (F. Bazzucchi).

http://dx.doi.org/10.1016/j.euromechsol.2017.07.008
0997-7538/

The actual common interest is focused on the interaction between different buckling modes for thin-walled structures (Schafer and Peköz, 1999), with particular regards to flexural, torsional and lateral coupling (Schafer, 2002), (Magnucka-Blandzi and Magnucki, 2011), (Dubina, 2001) and (Britvec, 2014).

At the same time, the increasing new interest in the design of smart devices has brought the possibility to take some advantages through the triggering of the buckling for such mechanical systems (Huet al, 2015). In many cases, buckling responses have certain benefits and are especially suitable for these smart applications. Buckling-induced instabilities are thus being increasingly explored and a large number of interesting prototypes in terms of structural forms and material uses have been proposed. Many applications are related to energetic uses such EH (Energy Harvesting) technologies (i.e. (Kim et al., 2011)) or to the realization of alternative sensory devices (Batra et al., 2007). Innovative prototypes that take advantage by the related buckling displacements regard the field of self-deploying and self-locking structures (Friedman and Ibrahimbegovic, 2013). Furthermore, buckling applications can be largely found in the design of smart materials, especially for the shape-changing (Huang et al., 2014) and shape-memory materials (Jani et al., 2014), (Danso and Karpov, 2017). All these studies opened a new branch of the Structural Instability research, but, at the same time, are based on its same methods and approaches.

In the present study, a theoretical evaluation, together with a numerical comparison, of the maximum load reduction for a simple structure is proposed (Bazzucchi et al., 2017): the Authors consider the snap-through of a compressed Von Mises Arch vs. the global and local elastic buckling of the same structural configuration by a direct equilibrium method. In (Bazzucchi et al., 2017) the theoretical fundamentals have been presented for a particular structural arrangement in terms of restraining conditions. The pinnacle result that has been obtained is the theoretical formulation of an *interaction curve*, that predicts the occurrence of the interaction between snap-through and buckling on the basis of inertial and geometrical properties (Fig. 1). A wide series of numerical simulations have been presented to support the theoretical evidences. In this work a step forward was accomplished, and two interaction and form indexes are presented to trigger or predict an interactive buckling. Accompanied to these indexes, the possibility of an easy evaluation of the load reductions and of the structural behavior is introduced. On one hand, the load reductions can be significant and the consequence of this phenomenon has a main importance in the safe design of structures. On the other hand, such phenomenon can be used as activation for a smart buckling-induced device. The interaction makes possible the realization of a threshold for the precise trigger of the snap-through (at the same level of internal stresses). The study of these phenomena can also be used as an interpretation to prevent the pull-in instability (Zhang et al., 2014), which is the uncontrolled buckling of a device, when a structure is affected by an amplification due to the possible interactive buckling.

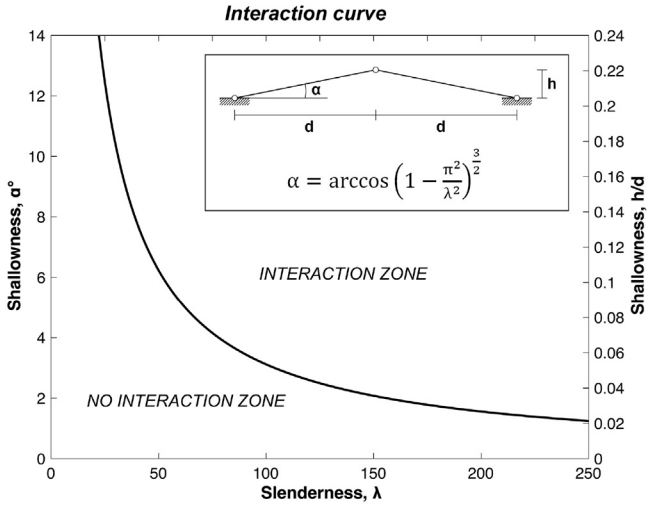

Fig. 1. Interaction curve for a Von Mises arch type structure.

Furthermore, the assembly of interaction domains, on the basis of the expected imperfections, is presented. According to this approach, it is possible to supply the most important tools for the problem of coupled instability (Gioncu, 1994): a theoretical method and a quantitative evaluation of the critical load reduction due to the presence of structural imperfections.

2. Definition of the model

A Von Mises Arch of semi-span $d = 2.5m$ and variable height h was considered as the basic structural model for the analyses (Fig. 2a). A set of ten tubular steel sections was used in order to realize different slendernesses λ for the system beams, as detailed in Fig. 2b. Ten $\frac{h}{d}$ values of the defined shallowness ratios were varied from 0.02 to 0.20, as indicated in Fig. 2c. In order to investigate the imperfections sensitivity of the structure, a geometrical defect was adopted through a sinusoidal configuration for the beam, which was identified by a midspan deviation e_0 from the line axis. It is necessary to distinguish between the two cases:

- *symmetric imperfection pattern*: the deviation is applied downward to each constituting beam of the arch as indicated in Fig. 2d. The entity of midspan deviation could be different for each beam ($e_{0,sx} \neq e_{0,dx}$), and the values used in the analyses were related to the length L of the beam, respectively equal to $\frac{L}{1000}$, $\frac{L}{300}$ or 0.
- *asymmetric imperfection pattern*: the imperfection is applied in a reverse direction for two adjacent beams (Fig. 2e). The same values of the symmetric imperfection pattern were used for the midspan deviations. The cases with a sole beam affected by a deviation are considered as asymmetric pre-deformed configurations.

The reason why it is necessary to distinguish these two patterns is that the pre-deformed configuration has an influence on the activation of the related buckling mode, which vary as the restraining conditions change. When the external and internal connections are realized with hinges, the beams are simply compressed and the global Eulerian buckling modes coincide with the ones of each bar (Fig. 3a). Because one bar can buckle independently from the other, in order to ignite the interaction it is the same if the deviation is applied upward or downward (Fig. 3b). On the contrary, if clamps are present as connections, every Eulerian buckling mode involves two adjacent beams (Fig. 3c and d). Then, a symmetric imperfection pattern will induce an interaction with the second Eulerian buckling mode, which is characterized by an higher critical load. As a consequence, the imperfection was applied once in a reverse direction for the adjacent beams, and another in the symmetrical form (Fig. 3e and f). Operating this way, the first and the second Eulerian eigenshapes are respectively considered to induce interaction. All the numerical analyses were conducted by a displacement control scheme, applying a vertical incremental displacement U at the crown node of the arch and evaluating the value of the vertical reaction F at the same node (ex. Fig. 4a). A FEM co-rotational formulation was implemented through the numerical Solver engine of LUSAS 15.1 and nonlinear BTS3 elements were

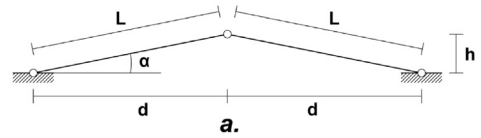

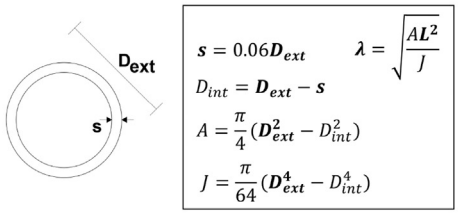

h [m]	h/d	λ
0.05	0.02	20
0.10	0.04	40
0.15	0.06	60
0.20	0.08	80
0.25	0.10	100
0.30	0.12	120
0.35	0.14	140
0.40	0.16	160
0.45	0.18	180
0.50	0.20	200

c.

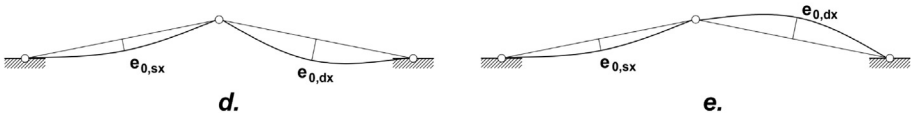

Fig. 2. a. The structural model: a Von Mises arch. **b.** Geometric characteristics of the tubular sections used for the arches. **c.** Shallowness ratios and slenderness sets used in the numerical analyses. **d.** symmetric imperfection pattern. **e.** asymmetric imperfection pattern.

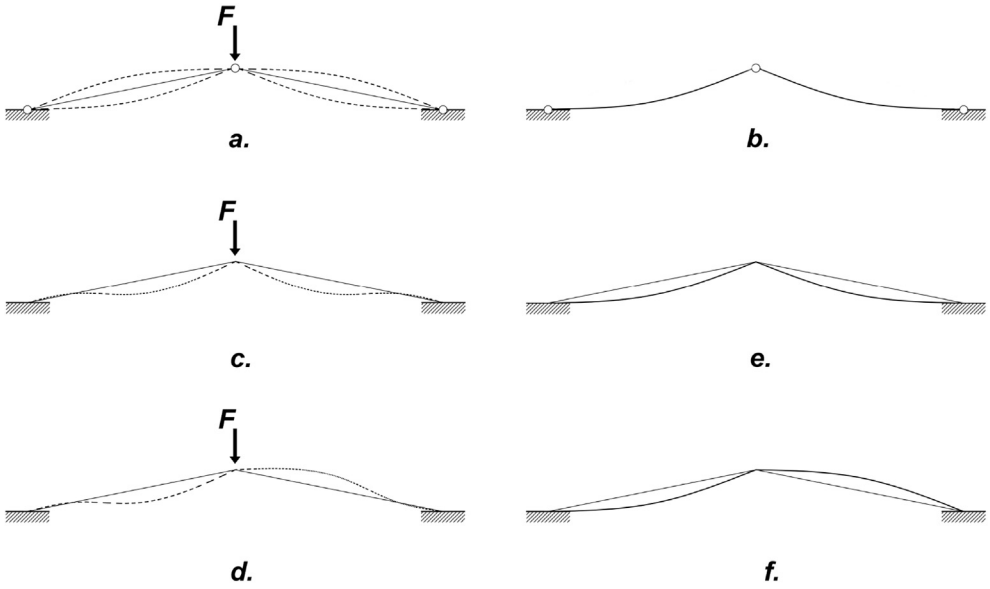

Fig. 3. a. Eulerian buckling eigenshapes of the hinged arch. **b.** Symmetric imperfection pattern for the hinged arch. **c.** Second and first (**d.**) Eulerian buckling eigenshape of the clamped arch. **e.** Symmetric and asymmetric (**f.**) imperfection patterns for the clamped arch.

used to build the model. The used number of finite elements was 40 for each bar; the step-by-step integration was carried through the Modified Newton-Rhapson method, with a convergence based on the maximum absolute residual and the residual RMS equal both to 1.0×10^8. The maximum number of iterations per step was equal to 12, and no step reduction was allowed. Iteration were started by a load factor equal to 2×10^{-2} of the applied displacement. For the successive steps, the maximum change in the load factor was set up to the value of 5.0×10^{-1}. Average total solving time was recorded in the range of 35 s.

3. Numerical simulations

3.1. Equilibrium paths for a clamped structural arrangement

A detailed treatment of the snap-through/Eulerian buckling interaction for a hinged system in presence of geometrical imperfections can be found in (Bazzucchi et al., 2017). The equilibrium path of the generic arch, when is subjected to this interaction, evidences a nonlinear bifurcation point along the primary equilibrium path (snap-through) in correspondence with the intersection of linear buckling branch of the single bar (Bazzucchi et al., 2017). As a consequence, every equilibrium path of the imperfect systems results to be enveloped by the bifurcated branch, and a limit point is always present along the $F - U$ curve (Bazzucchi et al., 2017). On the contrary, the existence of the snap-through phenomenon for a clamped arch is subjected to particular geometrical and inertial properties of the system (Rubin, 2004). The higher restraining degree expressed by this considered configuration, makes not possible for some cases (low values of λ and $\frac{h}{d}$) the occurrence of the snap-through in favor of an indefinite tension stiffening behavior. As an example of this transition, the changing in the structural

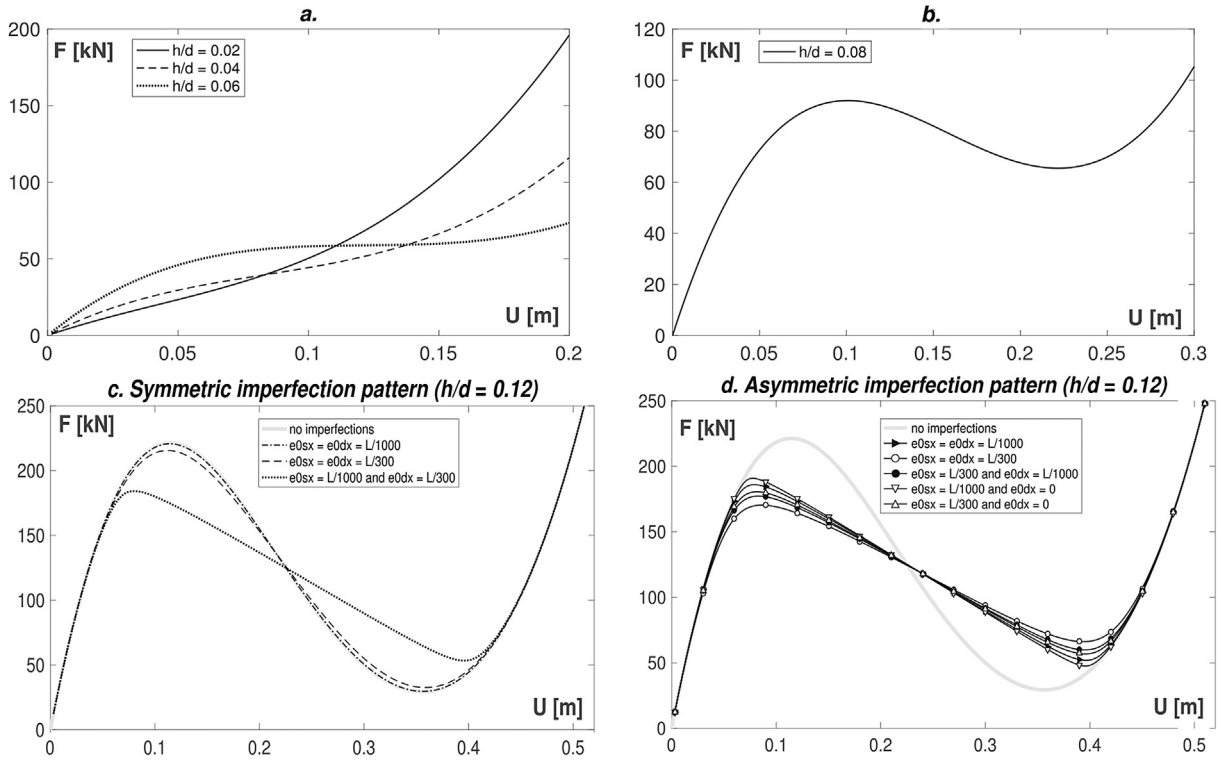

Fig. 4. a. Equilibrium path of the clamped arch with no imperfections and variable height. **b.** Equilibrium path for the $\frac{h}{d} = 0.08$. arch without imperfections **c.** Equilibrium path for the $\frac{h}{d} = 0.12$ arch with different symmetric imperfection patterns. **d.** Equilibrium path for the $\frac{h}{d} = 0.12$ arch with different asymmetric imperfection pattern.

responses for a variation of $\frac{h}{d}$ of a $\lambda = 80$ fixed arch were reported. $F - U$ curves up to $\frac{h}{d} = 0.06$ showed no limit point along them and a unique inflection point was instead present in correspondence to $U \simeq h$ (Fig. 4a). The snap-through phenomenon becomes evident from $\frac{h}{d} = 0.08$, however without any interaction occurrence. In (Fig. 4b), only the equilibrium path of the ideal system was reported, since the effect of imperfections was irrelevant for all the adopted schemes. Increasing the $\frac{h}{d}$ ratio, the shallowness of the structure decreases and as it has been observed for the hinged system (Fig. 1) the interaction started to appear. In Fig. 4c and d the $F - U$ curves in the case of $\frac{h}{d} = 0.12$ were reported. It can be observed how the equilibrium path of the symmetric imperfection pattern got influenced by a unique scheme (Fig. 4c), whereas all the asymmetric patterns caused a significant reduction of the critical load (Fig. 4d). In detail, when both the arch beams were affected by the same symmetric deviation, $e_{0,sx} = e_{0,dx} = L/1000$ or $L/300$, the interaction did not occur because the Eulerian buckling equilibrium path did not intersect the primary snap-through one. The scarce limit load reduction had to be only attributed to the presence of imperfections, which realized a weaker arch-like configuration than the one when both the constituting beams were rectilinear. At the same time, the case with $e_{0,sx} = L/300$ and $e_{0,dx} = L/1000$, even if both were applied downward on the basis of a symmetric eigenshape, the resultant equilibrium path showed a nonlinear bifurcation along the first Eulerian buckling mode. This means that the differential midspan deviation between the two constituting beams made the system behave more like an asymmetric configuration than a symmetric one. This significance will be more evident with the second example discussed later in this Section. In Table 1, the summary of the limit load values, and their reduction against the ideal system (without imperfections) were reported for every considered system. As mentioned before, it is interesting to note that the symmetric pattern with different midspan deviation implicated approximately the same reduction of an asymmetric pattern with a $L/1000$ geometrical defect.

A linearized Eulerian buckling analysis for the ideal arch gave back the values of the critical loads for the first two eigenshapes: $282kN$ for the first asymmetric mode and $552kN$ for the symmetric one. This means that, the first critical load of the arch is 25% greater than the snap-through limit load ($221.32kN$). Such load could be then safely considered as the collapse load condition if the two analyses were performed separately. However, the evaluation of the interaction phenomenon sheds light on a new critical situation, which arose when an imperfect system was considered. As can be observed in Table 1, the actual instability critical load is 23.02% lower than the ideal case evaluated with a nonlinear analysis.

In Fig. 5a and b the resultant equilibrium paths of the arch with $\frac{h}{d} = 0.16$ were reported. Even if the interaction was present with both the first two buckling modes, the more critic situation remained the pre-deformed arch with an asymmetric imperfection pattern (Fig. 5b). As can be seen in Table 2, the maximum load reduction reached almost the half of the perfect arch snap-through limit load.

Anyway, it is interesting to note that as in the previous case ($\frac{h}{d} = 0.12$), the symmetric pattern with a different midspan deviation between the 2 bars, produced a significant load reduction: its value is comparable to the generic one caused by an asymmetric pattern. All of this can be better appreciated through the comparison of the equilibrium paths related to the considered imperfection patterns (Fig. 5a and b). It is easy to see that the dotted line in Fig. 5a, corresponding to a deviation pattern with $e_{0,sx} = L/300$ and $e_{0,dx} = L/1000$ is much more similar to any of the equilibrium paths of the asymmetric pattern (Fig. 5b) than to one of the remaining two of the symmetric deviation scheme. This means, as above mentioned, that even if the deviations were applied both on the same direction (downward, as indicated in Fig. 3e), in this case the

Table 1
Load reduction for the $\frac{h}{d} = 0.12$ caused by different imperfection patterns in relation to the limit load of the corresponding perfect system.

		F [kN]	Load reduction [%]
no imperfections		221.32	–
symmetric pattern	$e_{0,sx} = e_{0,dx} = L/1000$	220.72	0.27
	$e_{0,sx} = e_{0,dx} = L/300$	215.56	2.60
	$e_{0,sx} = L/1000$ and $e_{0,dx} = L/300$	184.23	16.76
asymmetric pattern	$e_{0,sx} = L/1000$ and $e_{0,dx} = 0$	190.86	13.76
	$e_{0,sx} = e_{0,dx} = L/1000$	185.97	15.97
	$e_{0,sx} = L/1000$ and $e_{0,dx} = 0$	180.53	18.43
	$e_{0,sx} = L/1000$ and $e_{0,dx} = L/300$	177.22	19.93
	$e_{0,sx} = e_{0,dx} = L/300$	170.36	23.02

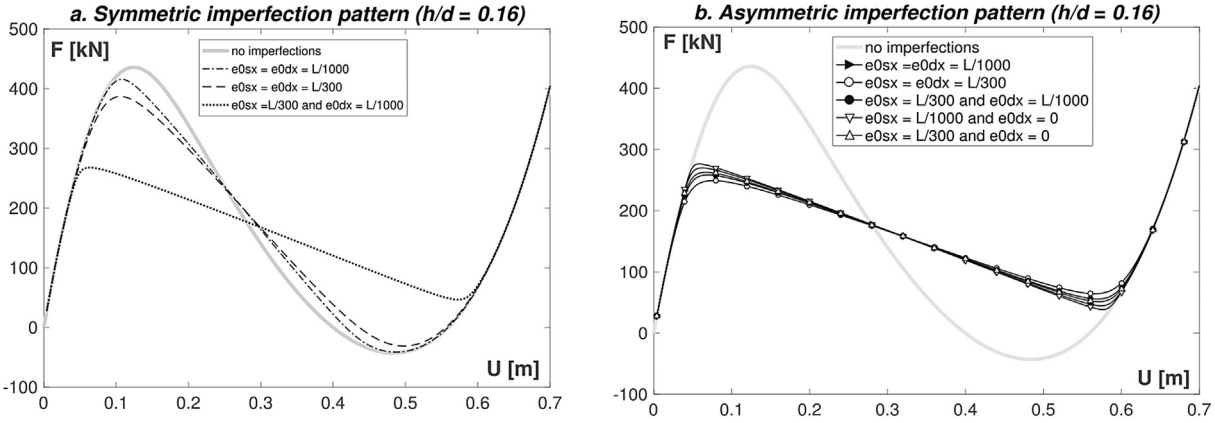

Fig. 5. a. Equilibrium path for the $\frac{h}{d} = 0.16$ arch with different symmetric imperfection patterns. **b.** Equilibrium path for the $\frac{h}{d} = 0.16$ arch with different asymmetric imperfection pattern.

Table 2
Load reduction for the $\frac{h}{d} = 0.16$ caused by different imperfection patterns in relation to the limit load of the corresponding perfect system.

		F [kN]	Load reduction [%]
no imperfections		435.76	–
symmetric pattern	$e_{0,sx} = e_{0,dx} = L/1000$	415.75	4.59
	$e_{0,sx} = e_{0,dx} = L/300$	386.86	11.22
	$e_{0,sx} = L/1000$ and $e_{0,dx} = L/300$	267.75	38.55
asymmetric pattern	$e_{0,sx} = L/1000$ and $e_{0,dx} = 0$	276.39	36.57
	$e_{0,sx} = e_{0,dx} = L/1000$	269.90	38.06
	$e_{0,sx} = L/300$ and $e_{0,dx} = 0$	262.69	39.72
	$e_{0,sx} = L/1000$ and $e_{0,dx} = L/300$	258.32	40.72
	$e_{0,sx} = e_{0,dx} = L/300$	249.07	42.84

interaction occurred through the nonlinear bifurcated branch of the asymmetric eigenshape. This is neither obvious or intuitive, because a symmetric imperfection scheme, even with different values for $e_{0,sx}$ and $e_{0,dx}$, implied that the entire initial structure was underneath the line axes of the perfect arch; the first linear buckling eigenshape expected instead an asymmetric vertical deviation (with respect to the pre-buckled line axes configuration) of the two constituting beams. The explanation of this occurrence is that the governing parameter that triggered the nonlinear bifurcation has to be detected in the *geometric similarity* between an imperfection pattern and the considered Eulerian eigenshape. To this purpose, a simple geometric entity Δ was defined as the vertical distance between the two constituting beams at the midspan level in the imperfect configuration (Fig. 6). It is possible to observe in Fig. 7 that Δ works better as a maximizer parameter of the load reduction due to imperfections: in this plot, the equilibrium paths of the system with $\frac{h}{d} = 0.16$ as a shallowness ratio were displayed for every imperfection pattern considered. Load reduction resulted to be proportional to Δ, evidencing that greater the distance between the two maximum deviations, lower the critical load of the system. Under these circumstances, the system with an asymmetric imperfection pattern and both the two deviations equal to $L/300$ resulted to be the one subjected to the highest load reduction. Surprisingly, the symmetric pattern characterized by the highest load reduction resulted to be underneath two of the asymmetric imperfection patterns (Fig. 7). This evidence has two main implications: the former suggests that the indiscriminate adoption of the highest deviation magnitude does not always lead to the lowest critical load (in this case, the higher load reduction of a symmetric pattern has been obtained with a $L/1000$ deviation for one of the two beams). The latter implies that when midspan deviations are used to simulate the imperfection scheme, its implementation to the elements can not be carried out by trying to retrace the absolute directions of the buckling eigenshape. The search for the imperfection pattern that minimizes the critical load has instead to be relied to parameters that can describe the maximum achievable geometric similarity between the imperfection scheme adopted and the weakest eigenshape. For a Von Mises arch-like structure,

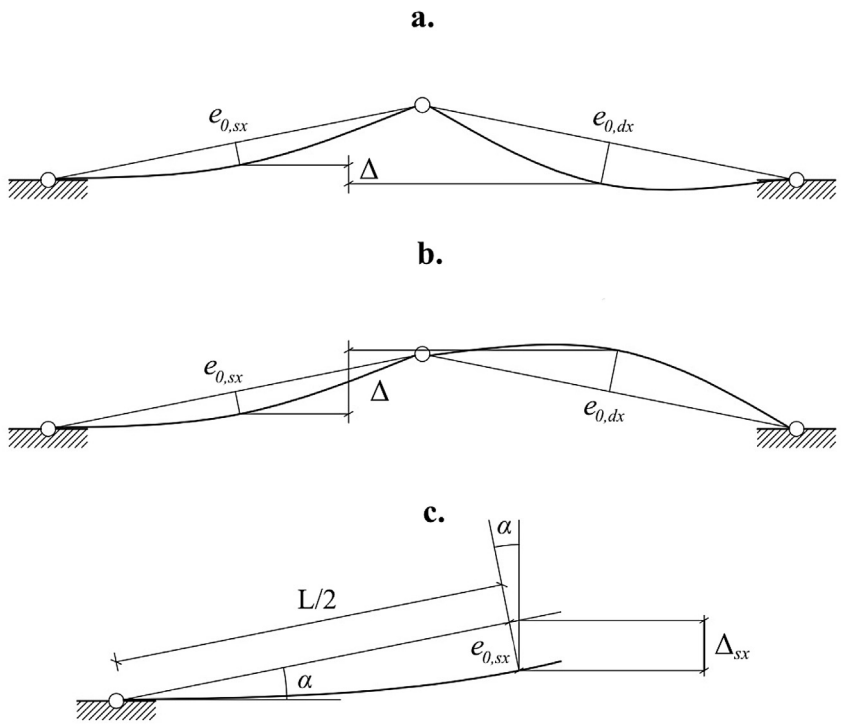

Fig. 6. Definition of the vertical distance Δ between the two beams with a symmetric (**a.**) and an asymmetric (**b.**) imperfection pattern. **c.** Geometric correlation between Δ and the generic midspan deviation e_0.

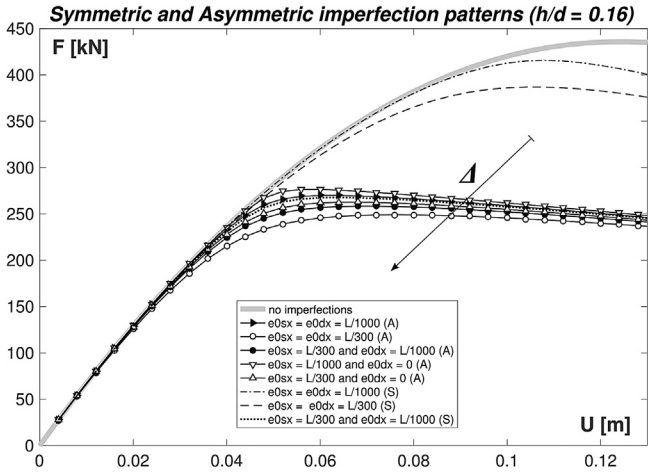

Fig. 7. Equilibrium paths for the $\frac{h}{d} = 0.16$ arch affected by the whole set of imperfection patterns (Asymmetric (A) and Symmetric (S)).

the defined Δ parameter is sufficient to describe this similarity. As detailed in Fig. 6, Δ can be derived by the sum of the projections of the midspan deviations along the vertical direction. The generic projection Δ_{sx} is connected to $e_{0,sx}$ by the relation:

$$\Delta_{sx} = \frac{e_{0,sx}}{\cos(\alpha)} = \frac{e_{0,sx}}{\cos\left[\arctan\left(\frac{h}{d}\right)\right]}, \tag{1}$$

that can be rewritten (Fig. 2a) as:

$$\Delta_{sx} = e_{0,sx}\sqrt{1+\left(\frac{h}{d}\right)^2}. \tag{2}$$

Then, through the simple addition $\Delta_{sx} + \Delta_{dx}$ the value of Δ is obtained for every given imperfection scheme. In Table 3, these values, expressed in *mm*, were reported in descending order for the considered imperfection patterns, confirming the trend of the equilibrium paths in Fig. 7. Furthermore, three geometric similarity indexes were evaluated to prove that an higher Δ value means an higher similarity degree between the imperfection pattern and the first buckling mode eigenshape (Fig. 8a). In detail, the first and second order of Minkowski metric ($_1d\mathbf{M}m$ and $_2d\mathbf{M}m$) together with the Chebyshev distance ($d\mathbf{C}$) were used to evaluate the average normalized (by the maximum buckled vertical deviation, assumed a unitary scale factor) distance from an imperfection pattern to the eigenshape (Wang et al., 2004). For example, the second order of Minkowski metric was evaluated between each node *j* of the first buckling eigenshape and the corresponding node *i* of the asymmetric pattern $e_{0,sx} = e_{0,dx} = L/1000$, as displayed in (Fig. 8b). Same evaluation was completed for every node *k* of the symmetric pattern $e_{0,sx} = L/1000$ and $e_{0,dx} = L/1000$. The average value of these quantities indicated how distant was the considered imperfection pattern from the fundamental eigenshape, working as *form diversity* indexes (Fig. 8c and d). Complementary of these indexes, $_{1M}I$, $_{2M}I$ and $_{C}I$, were used as similarity indicators and, as

Table 3
Δ factor and geometric similarity indexes for each considered imperfection pattern.

Imperfection pattern	Δ [*mm*]	$_{1M}I$	$_{2M}I$	$_{C}I$
$e_{0,sx} = e_{0,dx} = L/300$ (A)	17.09	381.4	461.0	468.0
$e_{0,sx} = L/300$ and $e_{0,dx} = L/1000$ (A)	11.11	379.9	459.3	466.2
$e_{0,sx} = L/300$ and $e_{0,dx} = 0$ (A)	8.55	379.2	458.5	465.4
$e_{0,sx} = L/300$ and $e_{0,dx} = L/1000$ (S)	5.98	378.6	457.8	464.7
$e_{0,sx} = e_{0,dx} = L/1000$ (A)	5.13	378.4	457.6	464.4
$e_{0,sx} = L/1000$ and $e_{0,dx} = 0$ (A)	2.56	377.7	456.8	463.7
$e_{0,sx} = e_{0,dx} = L/300$ (S)	0.00	377.1	456.1	462.9
$e_{0,sx} = e_{0,dx} = L/1000$ (S)	0.00	377.1	456.1	462.9

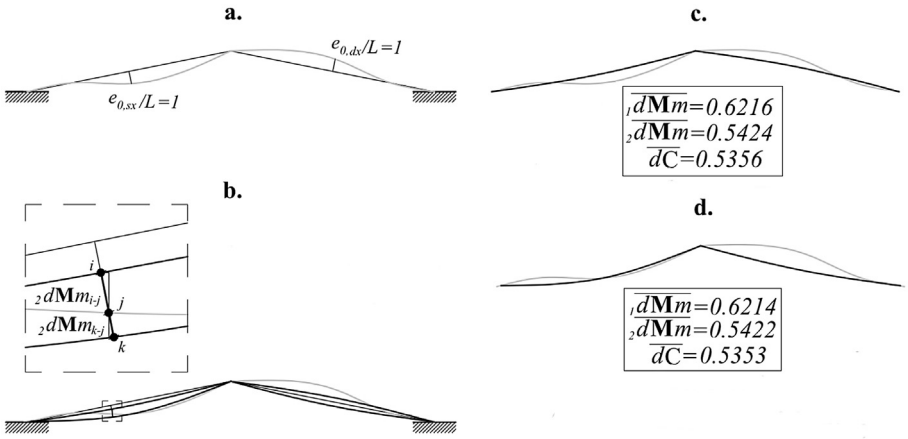

Fig. 8. a. Fundamental buckling eigenshape, normalized to the lengths of the beam. **b.** Distance between the generic node j of the buckling eigenshape and the corresponding node i and k of two considered imperfection patterns. Average distance indexes of the asymmetric imperfection pattern with $e_{0,sx} = L/1000$ and $e_{0,dx} = L/1000$ (**c.**) and the symmetric one with $e_{0,sx} = L/300$ and $e_{0,dx} = L/1000$ (**d.**).

predicted, the results are consistent with the definition of Δ, indicating that its highest value means the highest geometric correspondence degree to the minimum buckling load configuration. The symmetric imperfection pattern with $e_{0,sx} = L/300$ and $e_{0,dx} = L/1000$ resulted to be, even if not intuitively, more similar than the asymmetric configuration $e_{0,sx} = L/1000$ and $e_{0,dx} = L/1000$ to the first buckling eigenshape by a relative percentage, using $_{2M}I$, of 2% (Fig. 8c and d). It is important to reiterate that this indicator Δ, works better than the common parameters commonly used for modal correlation. Under these circumstances, it can be easily proved that *MAC* indicator (Allemang and Brown, 1982) would have produced an higher geometric similarity for the $L/1000$ asymmetric pattern than the differential symmetric $L/1000$ and $L/300$ one. It is evident that the symmetric imperfection pattern with the same deviation magnitude for the constituting beam was identified by a value of Δ equal to 0. Both the two considered patterns were obviously characterized by the same similarity index, that resulted to be the lowest one (Table 3) among the whole set.

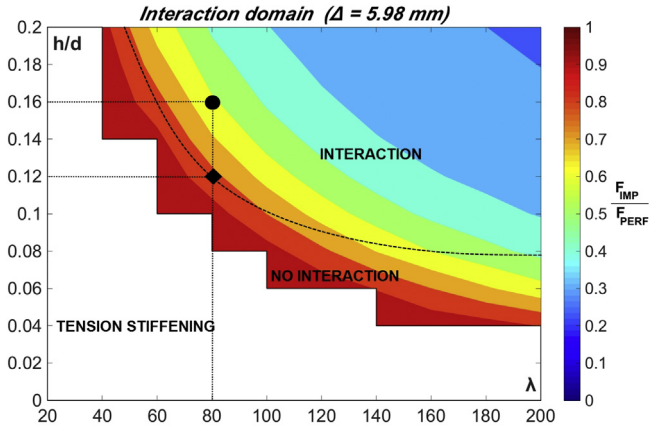

Fig. 9. Interaction domain of a clamped arch affected by a symmetric imperfection pattern with $e_{0,sx} = L/300$ and $e_{0,dx} = L/1000$. Contour plot shows the expected reduction in respect with the ideal geometric arrangement. Circle and diamond dots represent the analyzed systems in the previous section.

3.2. Interaction reductions domain

On the basis of the definition of Δ and the analyses that were conducted, it is possible to define the interaction domain, which predicts the expected load reduction due to an applied imperfection pattern. It can be done through the mapping of the ratio between the critical load of a system affected by a prescribed imperfection pattern and the corresponding one of a perfect arrangement. If this operation is conducted on a slenderness vs. shallowness ratio plane the combined information of interaction and reduction can be accomplished. For example, in Fig. 9, the interaction domain of the symmetric imperfection pattern characterized by $\Delta = 5.98mm$ ($e_{0,sx} = L/300$ and $e_{0,dx} = L/1000$) was reported. Three macro-zones of structural behavior can be recognized: two of them does not foresee the interaction phenomena. In these cases, the instability can occur only by a pure snap-through of the system; associated reduction have to be conferred to the sole different strength of the geometry arrangement. As previously shown, for particular configurations the structural behavior will resemble the fixed beam in flexure (*tension stiffening*). On the opposite, the dotted line in Fig. 9 separates the structural configurations for which the interaction can or cannot occur. The diamond dot represents the case with $\frac{h}{d} = 0.12$ and $\lambda = 80$, whose equilibrium path has been analyzed in detail as a first example (Fig. 4). Circle dot is instead connected to the case of $\frac{h}{d} = 0.16$ and $\lambda = 80$ (Fig. 5). As already demonstrated, for a fixed value of slenderness, maximum load reduction increases together with the ratio $\frac{h}{d}$. With the help of the domain, it can be stated that for such slenderness, load reductions could be up to 60% where shallowness ratio is high. Also, these same values of losses were obtained for the more slender system without any interaction phenomena. This means that, in this particular arrangement, the applied imperfection pattern weakened the system towards the sole snap-through instability. Fig. 10a shows the interaction domain of the asymmetric imperfection pattern characterized by $\Delta = 17.09mm$ ($e_{0,sx} = L/300$ and $e_{0,dx} = L/300$). It is interesting to note that the interaction curve moved left from the previous case ($\Delta = 5.98mm$). This means that the interaction phenomenon was anticipated for each same structural arrangement, and it is accompanied with a higher load reduction, as the contour plot shows. On the contrary, for the symmetric imperfection pattern $\Delta = 0.0$ and $e_{0,sx} = e_{0,dx} = L/1000$, the interaction curve was located more right at the domain. It may be concluded that, factor Δ it is not only an indicator of the expected load reduction, but also a riskiness parameter, in terms of instability interaction, of the structural configuration. As a final example, interaction domain of the hinged system was reported (Fig. 11). In this case, snap-through instability always occurs (Bellini, 1972), but can be triggered by interaction

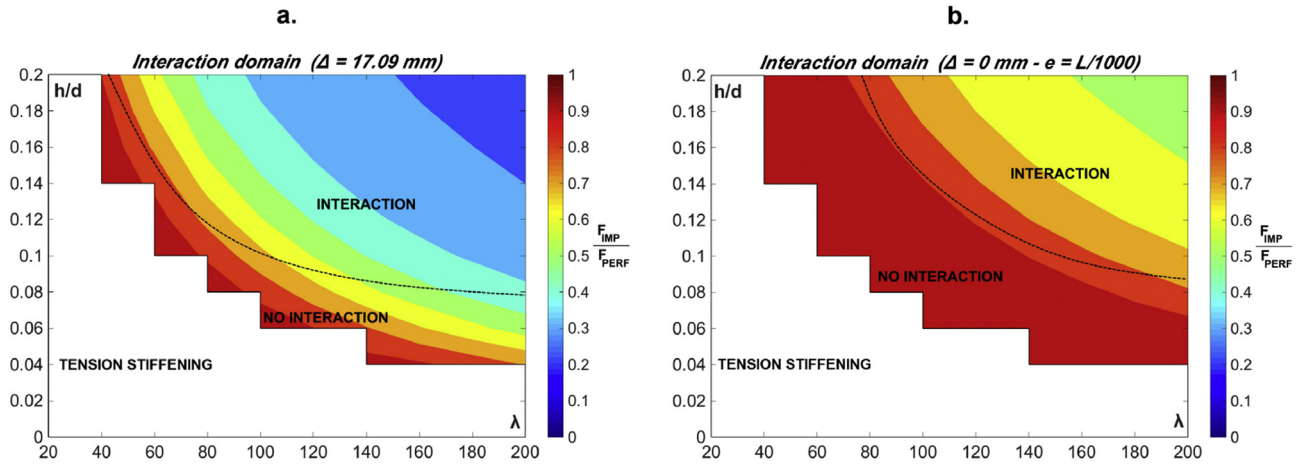

Fig. 10. a. Interaction domain of a clamped arch affected by an asymmetric imperfection pattern with $e_{0,sx} = L/300$ and $e_{0,dx} = L/300$. **b.** Interaction domain of a clamped arch affected by a symmetric imperfection pattern with $e_{0,sx} = L/1000$ and $e_{0,dx} = L/1000$ Contour plot shows the expected reduction in respect with the ideal geometric arrangement.

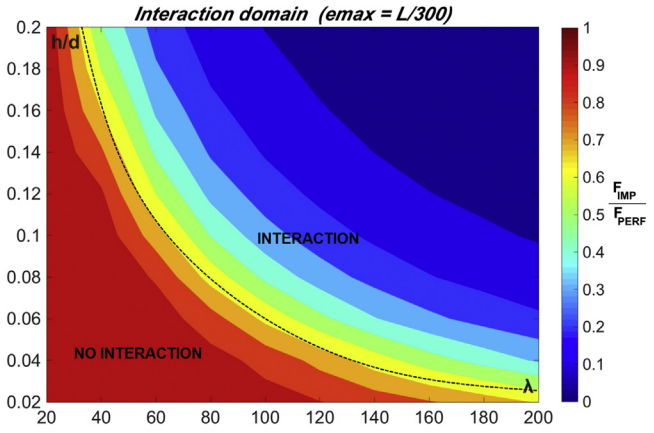

Fig. 11. Interaction domain of a hinged arch affected by an imperfection pattern with $e_{0,sx} = L/300$ and $e_{0,dx} = L/300$. Contour plot shows the expected reduction in respect with the ideal geometric arrangement.

with buckling when the structural system lays beyond the interaction curve (Bazzucchi et al., 2017). This curve, theoretically obtained in (Bazzucchi et al., 2017), if overlapped to the corresponding interaction domain, estimates a minimum load reduction of the 30%, due to the interaction, when compared to the ideal maximum load. In this restraining configuration, only the maximum deviation of one of the constituting beam drive the interaction (Bazzucchi et al., 2017), meaning that $\Delta = \frac{e_{0,sx}}{\cos(\alpha)} = 8.55mm$. Because this case represents the lowest position of the interaction curve, the Δ factor necessitates a reformulation that takes into account the restraining condition of the system.

4. Discussion

4.1. Generalized interaction domain

The factor Δ indicates the differential vertical deviation of the considered Von Mises arch system. As defined, it was able to predict the riskiness of a pre-deformed clamped configuration towards the interaction between snap-through and the first buckling eingenshape. Its nature, devoted to the interaction, was included in a more general *form factor* Ω, formulated as:

$$\Omega = \beta^2 \left[\frac{\Delta}{S} + \left(\frac{e_{max}}{S} \right)^2 \right], \tag{3}$$

where β takes into account the restraining conditions of the system through the multiplier of the generic member free length βL. S is the span of the structure get involved in the buckling phenomena: it means that it is equal to d (Fig. 2) when the eigenmode affects only one beam and $2d$ when the entire arch is buckled. e_{max} is the maximum midspan deviation among the ones that constitute the arrangement. Ω was evaluated for every imperfection pattern considered in the previous sections, and normalizing them to the largest one (hinged system affected by a $L/300$ imperfection), a decreasing trend was found, proportional to load reductions. As a consequence of what was mentioned earlier, Ω will be inversely proportional to the relative average distance, μ, between the interaction curve of a considered imperfection pattern and the one obtained theoretically for the hinged system. Obtained results were summarized in Table 4.

In Fig. 12 interaction curves of each considered imperfection pattern were reported, together with the related Ω factor. It is worth to note that, for a clamped configuration the interaction curve was obtained numerically by an exponential interpolation law of the interaction trail points in the following form:

$$\frac{h}{d} = a\lambda^{-b}, \tag{4}$$

where a and b were evaluated by a double second-order reverse regression. Obtained value for a and b are shown in Table 5 with

Table 4
Δ, Ω and μ factors for each considered imperfection pattern.

	Imperfection pattern	Δ [mm]	Ω	μ
hinged system	$e_0 = L/300$	8.55	1	–
	$e_0 = L/1000$	256	0.299	–
clamped system	$e_{0,sx} = e_{0,dx} = L/300$ (A)	17.09	0.252	0.07
	$e_{0,sx} = L/300$ and $e_{0,dx} = L/1000$ (A)	11.11	0.165	0.10
	$e_{0,sx} = L/300$ and $e_{0,dx} = 0$	8.55	0.127	0.11
	$e_{0,sx} = L/300$ and $e_{0,dx} = L/1000$ (S)	5.98	0.089	0.12
	$e_{0,sx} = e_{0,dx} = L/1000$ (A)	5.13	0.076	0.14
	$e_{0,sx} = L/1000$ and $e_{0,dx} = 0$ (A)	2.56	0.038	0.15
	$e_{0,sx} = e_{0,dx} = L/300$ (S)	0.00	$2.08E^{-4}$	0.45
	$e_{0,sx} = e_{0,dx} = L/1000$ (S)	0.00	$1.87E^{-5}$	0.48

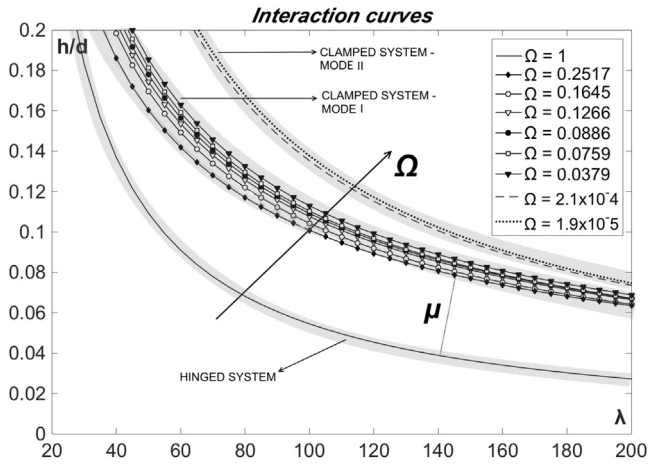

Fig. 12. Interaction curves for all the considered imperfection patterns. Every one of the them is represented by the corresponding Ω value. μ stays for the punctual distance from the considered interaction curve and the fundamental one (hinged system).

Table 5
Exponential laws parameters (a,b) for each interaction curve (identified by Ω). Because of the closed interaction curve equation for the hinged configurations, a and b were not reported for $\Omega = 1$ and $\Omega = 0.299$.

Ω	a	b
1	–	–
0.299	–	–
0.252	2.185	−0.668
0.165	2.634	−0.701
0.127	2.649	−0.696
0.089	2.8071	−0.705
0.076	2.989	−0.716
0.038	3.045	−0.715
$2.08E^{-4}$	7.746	−0.879
$1.87E^{-5}$	8.054	−0.884

respect to Ω. It can be observed that Ω and μ describe well the expected structural behavior towards the instability of the system.

Considering its definition, to each curve a load reduction value can be connected, and this value is the minimum one since the load reduction becomes higher as it moves beyond the interaction curve. In Fig. 13 these minima were reported for every interaction curve (identified by Ω). Is it possible to observe that, for a given buckling mode, the evaluated minimum load reduction had a unique value. This result allows to estimate the critical load of a system through the knowledge of the sole Ω factor. The nature of an interaction domain, indeed (see Fig. 11), suggests that every load reduction percentage belongs to a surface delimited by two exponential laws. It means that, in a 3D visualization, the contour plot stand for a surface, whose boundary lines are decreasing exponential laws. These lines can be obtained by the intersection of a plane parallel to the $\frac{h}{d} - \lambda$ plane Fig. 14. This gives an interpretation on why the two hinged configuration had the same interaction curve but different Ω factors. Observing Fig. 14, it can be seen that the intersection between the horizontal plane and the *reduction surface* defines the same interaction curve. It can be stated that the grade of the surface normal increases with the decreasing of Δ: when the interaction factor Δ is maximum, the surface normal is parallel to the $\frac{h}{d} - \lambda$ plane; once $\Delta \to 0$, the grade of the surface normal starts to increase, as in Fig. 14 was reported. This results allowed to divide the parameters that can intervene for the load reduction: the considered imperfection pattern and the structural configuration (restraining conditions included). This formulation was able to separate quantitatively, for the first time, the load reduction due to instability interaction, referred in literature as *first* and *second coupling erosion* (Gioncu, 1994).

Using a Ω -normalized vertical axis, a load factor $R = R(\Omega, \mu)$ can be defined to obtain the actual instability load of an imperfection pattern through a reduction multiplier as follows:

$$F_{cr} = RF_{perf}, \tag{5}$$

where, F_{perf} is the ideal critical load of the structural arrangement. For each of the analyzed cases, R factor coincides with the ratio mapped on the relative interaction domain (Figs. 9–11).

4.2. Parameters influence

The interaction domain and the load reduction factor R allow to draw out interesting remarks about the influence of the structural parameters. In Fig. 15a and b R was plotted vs. the slenderness λ and vs. the shallowness ratio $\frac{h}{d}$, as regard to $\Omega = 1$ structural configuration. These portrayals describe the projections of the interaction surface onto the vertical principal planes (Fig. 14). As can be seen from Fig. 15a/b, the more substantial imperfection influence on load reduction is present where the slenderness is high and the arch is not significantly deep. Anyway, load reductions greater than 50% of the perfect configuration were found for $\lambda < 100$ and average values of the arch rise (red dotted box in Fig. 15a). Interestingly, the $\lambda = 20$ system resulted to be always non-sensitive to structural imperfections; this result agrees with the definition of the interaction

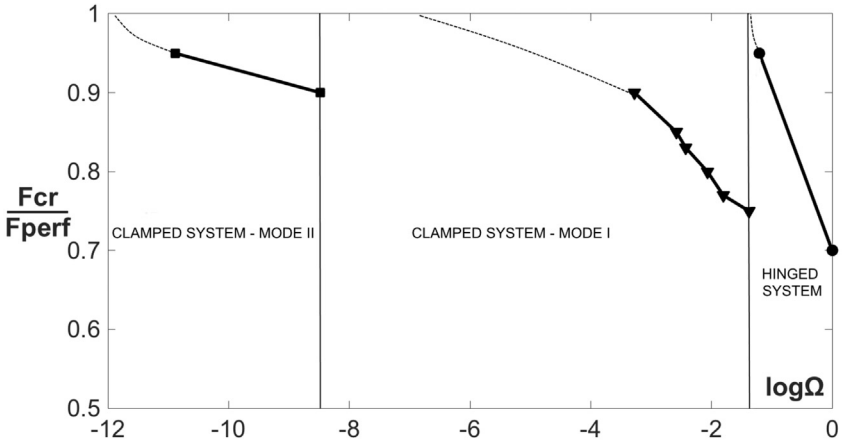

Fig. 13. Minima load reductions for every imperfection pattern in respect to the perfect configuration.

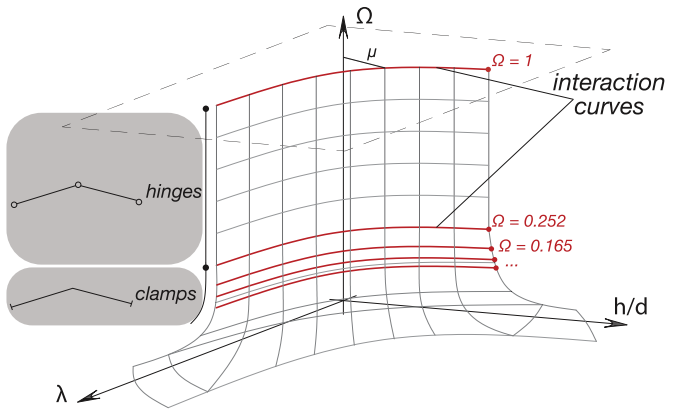

Fig. 14. Interactions surface. Ω axis defines the horizontal plane section to obtain the interaction curve of the considered structural configuration. Interaction curves from $\Omega = 0.252$ to 1 are equal, because represents the hinged arch. For $\Omega < 0.252$ clamped configurations are identified; the interaction curve increases its distance from the vertical axis because the interaction phenomena is retarded by the higher degree of restraining conditions.

curve, because it never intersect the vertical line $\lambda = 20$ Fig. 1 or Fig. 11. Interesting representations are offered by Fig. 15c and d. In this case, the influence of the imperfections magnitude was evaluated by plotting the ratio between two different R factors vs. λ and $\frac{h}{d}$. In this case, the two imperfection patterns of the hinged arch were considered, meaning that $R_{\Omega=1}$ and $R_{\Omega=0.252}$ were used. Observing Fig. 15c it can be see that each *differential reduction curve*, identified by $\frac{h}{d}$, constitutes of two parts: a decreasing one and a constant trend portion. For the former one, interaction did not occurred, and the load reduction increases as the imperfection magnitude becomes higher. The latter represents the curve portion for which the interaction occurred. Its constant trend suggests that the imperfection magnitude effect did not depend on the slenderness. Furthermore, as $\frac{h}{d}$ increases, the absolute value of the imperfection becomes less significant since the differential reduction settle for higher ratios. In these latter cases, only a 10% difference on the load reduction exists between the two considered imperfection pattern, even if their magnitude was substantially different ($L/300$ midspan deviation against $L/1000$). Fig. 15d makes easier to appreciate better this important remarks. The differential reduction ratio was plotted against $\frac{h}{d}$ for each λ curve. Where the interaction is not present, the effect of the imperfection magnitude is stronger as the rise of the arch increases. On the contrary, once the interaction occurred, the curves lays on the same envelope line. This results confirms the non-dependency on the slenderness, and that the amplitude of the imperfections becomes negligible for high arches. Discussed plots are related to the hinged models, anyway the same trend can be observed for the clamped systems. It may be concluded that, the shape prevails over the magnitude to activate the interaction. Under the light of this, Ω factor fulfills the aim of instability describer, since its nature is completely devoted to both *form* and *instability*.

4.3. Applications

Possible applications of this approach cover the entire field of

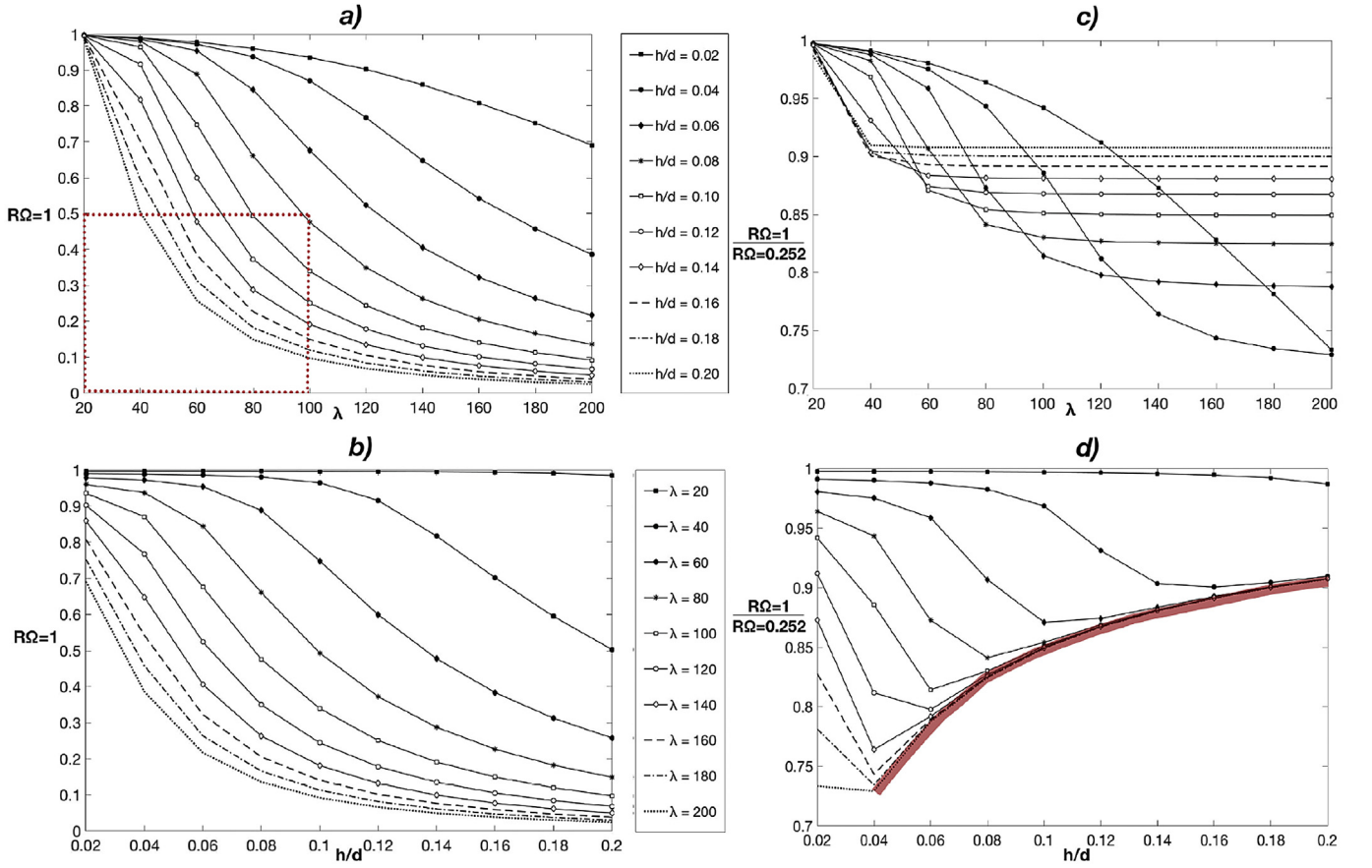

Fig. 15. Parameters influence on the expected load reductions. **a., b.** Hinged system affected by $L/300$ ($\Omega = 1$) imperfection pattern reduction ratios. **c., d.** Differential reduction between $L/300$ ($\Omega = 1$) and $L/1000$ ($\Omega = 0.252$) imperfection patterns.

structures in which the interaction between instability phenomena represent the principal design scenario. At building scale, shallow-dome structures and grid shells are the main interested typologies, since form finding design occupies a fundamental part in the planning process. Model defined in Section 2 is a simple but representative model for arch-like structures, and it can be expanded to more articulated systems without loosing its generality. However, the importance of this interaction (Δ) and form (Ω) factors domain approach appears reasonably strong and useful for the design and the characterization of buckling induced technologies. For example, a Von Mises arch-like sensor (Friedman and Ibrahimbegovic, 2013) could be arranged following a desired load reduction in order to have different trigger thresholds. At the same time, a shape identification could predict potential imperfections induced collapses, excluding sensor malfunctions or damages.

5. Conclusions

Theoretical foundations of this study have been presented by the Authors in another manuscript (Bazzucchi et al., 2017), in which the interaction curve of the Von Mises arch has been originally obtained. As a continuation, the presented work investigates on the structural behavior of shallow structures vulnerable to interaction between buckling and snap-through, with regards to different restraining conditions and imperfection patterns. The adopted structural model is a simple but complete non-linear geometrically structure, as defined in Section 2. Copious numerical analyses have been conducted by using a displacement control scheme together with FEM + Matlab engines (Bazzucchi et al., 2017). It has been found that, to have a full understanding on the interaction with the higher buckling modes, the more dangerous imperfection pattern has to be evaluated with proper *interaction factors*. To this purpose, the definition of a new Δ parameter made possible to identify completely the geometrical defects configuration to induce a certain buckling interaction with a corresponding load reduction. It has been demonstrated how the use of a consolidated parameters like *MAC* could lead to erroneous maximum load reductions, because only the buckling eigenshapes (or their combinations) could not outperform the more burdensome imperfection pattern arrangement.

Nonlinear numerical analyses results have been summarized in useful tools, defined as interaction domains. Their redaction, has allowed to estimate if a structural configuration has encountered the interaction and the consequential maximum load reduction through the distance μ from the interaction curve.

Interaction domains has been integrated to a unique 3D surface that described correctly the obtained results of the nonlinear numerical analyses. The interaction surface can be described with a form factor Ω that have been introduced in order to take into account the different restraining conditions and the considered imperfection pattern. Finally, a load reduction factor $R(\Omega, \mu)$ has been defined. In Section 4.1, has been shown how it can be used to predict the critical load of the structural model only by the identification of its form, that includes imperfection. Possible applications of this approach has been suggested in Section 4.3, and they cover structural form finding, monitoring, identification and sensors design.

References

Allemang, R.J., Brown, D.L., 1982. A correlation coefficient for modal vector analysis. In: Proceedings of the 1st International Modal Analysis Conference, vol. 1. SEM, Orlando, pp. 110–116.

Batra, R., Porfiri, M., Spinello, D., 2007. Review of modeling electrostatically actuated microelectromechanical systems. Smart Mater. Struct. 16 (6), R23.

Bazzucchi, F., Manuello, A., Carpinteri, A., 2017. Interaction between snap-through and eulerian instability in shallow structures. Int. J. Non-Linear Mech. 88, 11–20.

Bellini, P.X., 1972. The concept of snap-buckling illustrated by a simple model. Int. J. Non-Linear Mech. 7 (6), 643–650.

Bleich, F., 1952. Buckling Strength of Metal Structures. McGraw-Hill.

Bradford, M.A., Hancock, G.J., 1984. Elastic interaction of local and lateral buckling in beams. Thin-Walled Struct. 2 (1), 1–25.

Britvec, S.J., 2014. The Stability of Elastic Systems: Pergamon Unified Engineering Series. Elsevier.

Chilver, A., 1967. Coupled modes of elastic buckling. J. Mech. Phys. Solids 15 (1), 15–28.

Danso, L.A., Karpov, E.G., 2017. Cusp Singularity-based Bistability Criterion for Geometrically Nonlinear Structures. Extreme Mechanics Letters.

Dubina, D., 2001. The ecbl approach for interactive buckling of thin-walled steel members. Steel Compos. Struct. 1 (1), 75–96.

Friedman, N., Ibrahimbegovic, A., 2013. Overview of highly flexible, deployable lattice structures used in architecture and civil engineering undergoing large displacements. YBL J. Built Environ. 1 (1), 85–103.

Gioncu, V., 1994. General theory of coupled instabilities. Thin-Walled Struct. 19 (2–4), 81–127.

Gioncu, V., Balu, N., Dubina, D., Moldovan, A., Pacoste, C., 1992. Coupled instabilities in monosymmetrical steel compression members. J. Constr. Steel Res. 21 (1), 71–95.

Grimaldi, A., Pignataro, M., 1979. Postbuckling behavior of thin-walled open cross-section compression members. J. Struct. Mech. 7 (2), 143–159.

Huang, W.M., Lu, H.B., Zhao, Y., Ding, Z., Wang, C.C., Zhang, J.L., Sun, L., Fu, J., Gao, X.Y., 2014. Instability/collapse of polymeric materials and their structures in stimulus-induced shape/surface morphology switching. Mater. Des. 59, 176–192.

Hu, N., et al., 2015. Buckling-induced smart applications: recent advances and trends. Smart Mater. Struct. 24 (6), 063001.

Jani, J.M., Leary, M., Subic, A., Gibson, M.A., 2014. A review of shape memory alloy research, applications and opportunities. Mater. Des. 56, 1078–1113.

Kim, H.S., Kim, J.-H., Kim, J., 2011. A review of piezoelectric energy harvesting based on vibration. Int. J. Precis. Eng. Manuf. 12 (6), 1129–1141.

Koiter, W.T., 1970. The Stability of Elastic Equilibrium. tech. rep., DTIC Document.

Koiter, W.T., 1976. General Theory of Mode Interaction in Stiffened Plate and Shell Structures. tech. rep.. Delft University of Technology, Delft, The Netherlands. Technical Report Rept. WTHD-91.

Magnucka-Blandzi, E., Magnucki, K., 2011. Buckling and optimal design of cold-formed thin-walled beams: review of selected problems. Thin-Walled Struct. 49 (5), 554–561.

Maquoi, R., Massonnet, C., 1976. Interaction between Local Plate Buckling and Overall Buckling in Thin-walled Compression Members Theories and Experiments. Springer.

Rubin, M., 2004. Buckling of elastic shallow arches using the theory of a cosserat point. J. Eng. Mech. 130 (2), 216–224.

Schafer, B., 2002. Local, distortional, and euler buckling of thin-walled columns. J. Struct. Eng. 128 (3), 289–299.

Schafer, B., Peköz, T., 1999. Laterally braced cold-formed steel flexural members with edge stiffened flanges. J. Struct. Eng. 125 (2), 118–127.

Thompson, J., 1972. Optimization as a generator of structural instability. Int. J. Mech. Sci. 14 (9), 627–629.

Wang, Z., Bovik, A.C., Sheikh, H.R., Simoncelli, E.P., 2004. Image quality assessment: from error visibility to structural similarity. IEEE Trans. image Process. 13 (4), 600–612.

Zhang, W.-M., Yan, H., Peng, Z.-K., Meng, G., 2014. Electrostatic pull-in instability in mems/nems: a review. Sensors Actuators A Phys. 214, 187–218.